Cement and Concrete Composites 145 (2024) 105355

Contents lists available at ScienceDirect

Cement and Concrete Composites

journal homepage: www.elsevier.com/locate/cemconcomp

Healing capacity of Ultra High Performance Concrete under sustained through crack tensile stresses and aggressive environments

Bin Xi [a,*], Zhewen Huang [a], Salam Al-Obaidi [a,b], Liberato Ferrara [a,**]

[a] Department of Civil and Environmental Engineering, Politecnico di Milano, Piazza Leonardo da Vinci 32, Milano, Italy
[b] Roads and Transportations Engineering Department, University of Al-Qadisiyah, Diwaniyah, 58001, Iraq

ARTICLE INFO

Keywords:
UHPC
Self-healing
Durability
Load effect
Aggressive environments

ABSTRACT

This study investigates the self-healing capabilities of Ultra-High Performance Concrete (UHPC) under the combined influence of mechanical and environmental factors. Specifically, it delves into the long-term self-healing process in pre-cracked UHPC samples that endure continuous sustained tensile stresses across the cracks and are exposed to aggressive environmental conditions for one year. The results reveal that UHPC with narrow cracks exhibits a higher degree of self-healing, especially when exposed to tap water, where its self-healing capacity is most pronounced and improves with extended exposure. Furthermore, these self-healing mechanisms contribute to the restoration of mechanical properties and prevent chloride ion penetration by sealing the cracks. While a reduced level of self-healing is observed in saltwater and geothermal water exposure, prolonged exposure mitigates the inhibitory effect of aggressive ions on self-healing. SEM and EDS results provide evidence that samples subjected to extended exposure to salt and geothermal water exhibit a substantial presence of self-healing product-$CaCO_3$. This study not only emphasizes that pre-cracked UHPC, when exposed to both mechanical stresses and aggressive environments, can maintain excellent durability and mechanical strength due to its self-healing effect but also lays the foundation for evaluating the self-healing potential of cement-based materials under conditions representative of real-world structural scenarios. This is essential for advancing the integration of self-healing advantages into design concepts and performance-based verification approaches.

1. Introduction

Durability and sustainability are essential themes within contemporary civil engineering and construction industries. They have a direct impact on the longevity of structures and maintenance costs [1–3]. Concrete, a brittle material, is prone to cracking under tensile forces, leading to durability issues. Coastal concrete structures, for instance, are at risk of seawater-induced chemical penetration and reinforcement corrosion, resulting in concrete cracking and spalling.

As renewable energy sources gain prominence, new structural challenges arise. Notably, the corrosion of cementitious materials due to geothermal water becomes a significant concern, especially in regions like central and southern Italy, where infrastructure plays a crucial role in harnessing geothermal energy resources [4–6]. The geothermal water contains high levels of sulfate ions, and these aggressive environments reduce the performance and safety of the structure, increase repair and maintenance costs, and potentially lead to structural failure. Therefore, the search for more durable materials and improved concrete performance to reduce cracking and prevent chemical attack has become a hot topic. Furthermore, this necessitates the development and validation of performance-based durability design methodologies to consistently factor in the actual advantages offered by these advanced materials. This shift away from the prevailing "deemed to satisfy" prescriptive approaches, primarily reliant on material composition, currently dominating structural design codes, is imperative in addressing these challenges effectively.

Ultra High Performance Concrete (UHPC) is an innovatively consolidated composite material composed of cement, fine aggregates, and fibres. It is engineered to achieve a dense internal structure and superior mechanical properties, particularly in terms of compressive strength, tensile deformation and energy dissipation capacity [7–10]. According to ACI Committee 239 [11], UHPC can achieve a compressive strength higher than 150 MPa at 28 days, significantly higher than conventional concrete. Moreover, UHPC exhibits a one-of-a-kind tensile

* Corresponding author.
** Corresponding author.
E-mail addresses: bin.xi@polimi.it (B. Xi), liberato.ferrara@polimi.it (L. Ferrara).

https://doi.org/10.1016/j.cemconcomp.2023.105355
Received 3 May 2023; Received in revised form 7 November 2023; Accepted 9 November 2023
Available online 14 November 2023

strain hardening response with a tensile strength in the range of 8–10 MPa and a tensile strain capacity exceeding 0.2 % (yield strain of steel) when the appropriate dosage of fibres is added [12,13]. The stable multiple cracking of UHPC helps limit the width of each crack to 0.02–0.03 mm in use phase scenarios [14,15].

Numerous studies have shown that the denser internal structure of UHPC allows for higher durability [16–20]. However, concrete cracking is unavoidable, even for UHPC and especially in the service condition, where structures are often subjected to multifold actions including mechanical loads, temperature and humidity changes, shrinkage and creep deformation and environmental actions including chemical attacks, which can cause cracks to form. When cracked UHPC is further exposed to a harsh environment, harmful ions from the surroundings can infiltrate through these cracks, leading to the deterioration of both the cement matrix and the fibre reinforcement. This can result in substantial degradation of UHPC and compromise its overall material characteristics, thereby limiting its ability to fully leverage its high-performance potential. Although some studies have focused on changes in the long-term durability of UHPC [21–23], there has been little research concerning the development of the durability of cracked UHPC under sustained load conditions. In contrast to ordinary (reinforced) concrete, where tensile properties are often overlooked in the design process, the ability of UHPC to maintain these properties over time is a critical factor for its application. Tensile properties are a defining design parameter in UHPC applications, and their continued preservation is vital for ensuring structural durability, intended as the structure's ability to maintain the required level of performance throughout its intended service life and under expected structural service conditions.

The self-healing properties of UHPC are also a crucial factor influencing its durability. Due to the low water-cement ratio, UHPC has an inborn autogenous self-healing capacity [24–30]. The formation of cracks in UHPC can activate its self-healing mechanism, through enabling water to penetrate the material and close the cracks by producing certain chemical products. This process helps to slow down the penetration of external aggressive media. In addition, some "stimulating" self-healing techniques have been used in UHPC, further promoting the self-healing reactions and eventually repairing damaged parts of the material [27]. For examples, Ahn et al. [31] prepared UHPC with 20 % Fly Ash (FA) and 7 % Silica Fume (SF) and a water/binder (w/b) of 0.26. After exposure to water for seven days, it was observed that the healing products could effectively fill cracks that had a width of less than 100 μm. In the presence and absence of silicate-modified calcium oxide-based expansive agents (SCEA), Wang et al. [32] conducted a comparative analysis of UHPC with a w/b of 0.2, and found that the samples containing SCEA demonstrated a significant reduction in crack width, from 180 μm to 70 μm. Lo Monte and Ferrara [33] suggested UHPC samples containing slag exhibited improved recovery of bending performance after up to six months of water exposure, which was attributed to more active hydration reactions of slag particles at a later age.

To better understand the long-term durability mechanism of UHPC, it is crucial to consider the effect between the aggressive ions in the environment and the self-healing mechanism under mechanical load cracked state. This information is essential for establishing theoretical models and developing specification standards. The author previously summarized the effect of exposure environment on the self-healing performance of UHPC [27]. The previous research has rarely referred to the evolution of self-healing performance under the influence of both aggressive environment and loading. This paper aims to investigate the efficacy of the self-healing mechanism of pre-cracked UHPC in aggressive environments over a one-year period under sustained loading generating through-crack tensile stresses. The test samples were immersed in tap water, geothermal water and salt water, and the self-healing performance was evaluated using ultrasonic pulse velocity (UPV) tests, image processing techniques and Double Edge Wedge Splitting (DEWS) tests. Besides, a tailored set-up was designed, which enabled the sustained through crack tensile stress to be applied all along the examined exposure time. The morphology of the self-healing products was observed and idented using scanning electron microscopy (SEM) equipped with energy-dispersive X-ray spectroscopy (EDS). The study highlights that pre-cracked UHPC under both mechanical and aggressive environments can maintain high durability and mechanical strength because of self-healing effect. It also paves the way for the assessment of the self-healing capacity of cement-based materials under conditions which represent through structural service scenarios. Such assessments are crucial for integrating the advantages of self-healing into design concepts and performance-based verification approaches.

2. Materials and test methods

2.1. Materials

Table 1 displays the mix proportions of the UHPC employed in this study. The ratio of w/b (CEMI + slag) was 0.18 in order to create a dense and strong matrix. Moreover, 0.8 % by weight of crystalline admixture (Penetron Admix ®) was employed as a healing stimulator. The inclusion of crystalline admixture effectively enhances the healing capacity in concrete [34–37]. To gain tensile hardening properties, 1.5 % volume of straight steel fibers with l_f = 20 mm and d_f = 0.22 mm (Azichem Readymesh MR 200 ®) were employed. Earlier researches by the authors [38–40] give additional details about the mix composition and pouring procedure.

2.2. Preparation of the pre-cracking and sustained samples

The experimental samples were cut from in-situ-fabricated slabs [4]. They were stored in a laboratory environment (RH = 90 %, T = 20 °C) for one year to reduce the effect of late hydration of the slag on the assessment of self-healing property. After cutting the thin plates into square specimens, the square specimens were precisely shaped into DEWS samples. The shape of DEWS is shown in Fig. 1.The thickness is 30 mm and more information can be found in Ref. [38]. The DEWS test serves as an indirect tensile test method that has been shown to be an effective way to the straightforward identification of the tensile stress vs. Crack Opening Displacement (COD) constitutive relationship [41,42]; it is simple, clear and does not require back analysis, which is typically needed to determine the tensile constitutive relationship from bending test results.

To start with, the DEWS samples were intentionally pre-cracked. Two Linear Variable Differential Transformers (LVDTs) on either side of the sample were installed, as shown in Fig. 2. The aim was to achieve two average COD values, specifically 0.1 COD mm for narrow crack openings and 0.3 COD mm for wider ones. The choice of COD was based on previous research findings to facilitate future comparative studies [27]. The loading was halted and the maximum force was recorded when the average COD reached the specified value (around 0.1 mm/0.3 mm).

To subject the pre-cracked DEWS specimens to sustained through-crack tensile stress, a custom load-holding device was designed, as shown in Fig. 3. The device includes four bolts, four adjustable metal plates (15 × 1.5 × 2.5 cm), two steel bars 100 mm long and 10 mm in diameter, and nuts.

Initially, the pre-cracked specimen was centred in the device, and the

Table 1
Mixture proportion of UHPC.

Constituents (kg/m^3)						
CEM I 52,5 R	Slag	Water	Steel fibers	Sand 0–2 mm	Superplasticizer	Crystalline Admixture
600	500	200	120	982	33	4.8

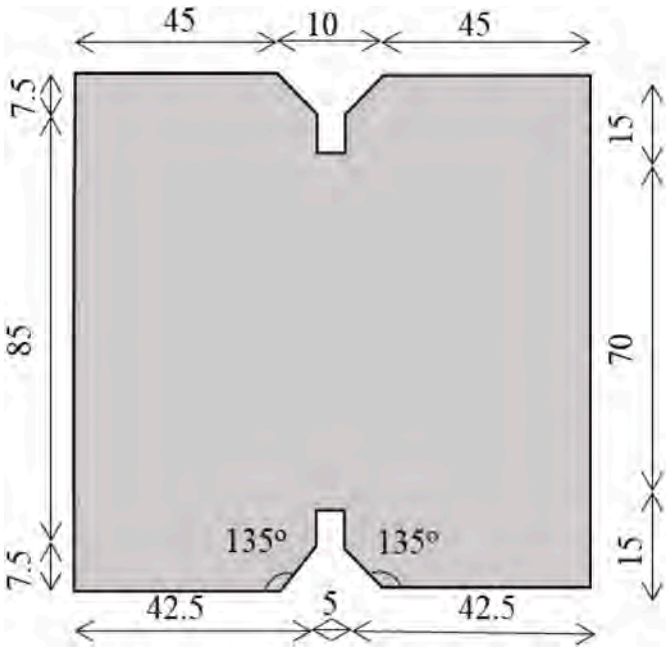

Fig. 1. Shape and dimensions of Double Edge Wedge Splitting test specimens. (Unit mm).

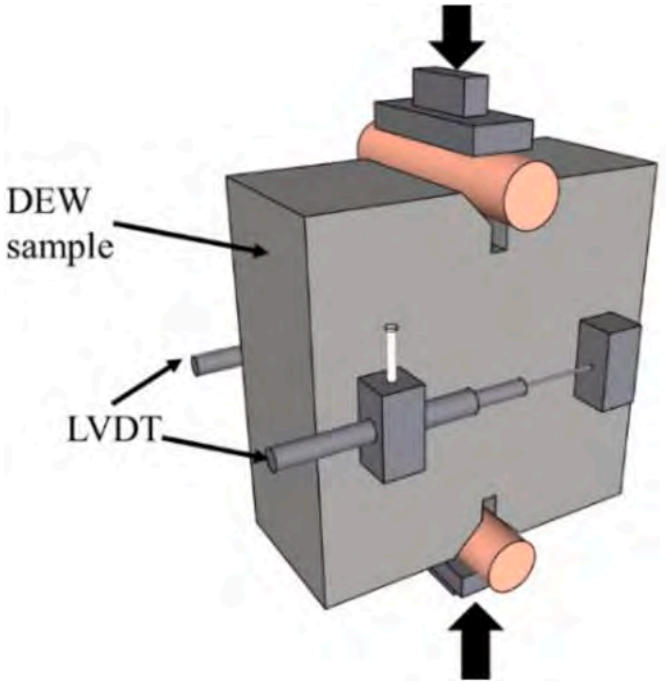

Fig. 2. Test set-up of DEWS tests.

top nuts were loosened while the bottom nuts were fastened. Next, the sample was subjected to compressive loading with the same speed of the pre-cracking test. The load applied to the sample matched the force recorded during pre-cracking at the desired COD value. Once the target load was attained, the "hold" button on the control console of the compression machine was pressed to maintain the force. The force was transferred to the metal plates which then forced the bolts through. Due to the adjustment of the top nuts on the bolts, the force was transmitted back to the specimen via the plates and bars, while the control screen showed that the load was decreasing. Once the reading values dropped to zero, the specimen was fully loaded up, and the device was locked. The entire re-loading testing procedure was completed within 5–10 min.

After being "submitted" to the sustained load as described above, the samples were subjected to three exposure conditions: tap water, salt water (with a sodium chloride concentration of 3.3 %), and geothermal water sourced from a water tank in the cooling tower of a geothermal power plant in Chiudino, Tuscany. The geothermal water exhibited high levels of sulphates and chlorides, as shown in Table 2 [4,18,43].

The cracked and uncracked reference samples were exposed to three environments and four different exposure times were set: 1 month, 3 months, 6 months and 12 months to investigate the evolution of self-healing properties at different times. Fig. 4 shows the test protocol and the number of samples. In each working condition, there are two samples. For example, two samples with a 0.1 mm COD were exposed to water for three months.

2.3. Microscope imaging techniques for the closure of cracks

The DinoLite digital optical microscope and its software, DinoLite Capture, were employed to record images of cracks in each sample to investigate the closure of the cracks. Since each image only recorded a small section of the crack, multiple images of the same crack were combined using Photoshop® to recreate the whole crack picture [38,44]. Fig. 5 illustrates the reconstructive procedure. Digital microscope images were taken at the beginning and at the end of each healing period. The reconstructed crack area, A_{crack}, was obtained using Photoshop's magic wand tool to select and measure the area of the crack, while the crack length, l_{crack}, was determined with Photoshop's measurement tool [44]. The average crack width, W, was obtained by dividing A_{crack} by l_{crack}. To evaluate the self-healing capability, an index of crack self-sealing (ICS) was established and calculated using Eq. (1).

$$Index\ of\ crack\ self\ sealing = \frac{W_{initial} - W_{after\ sealing}}{W_{initial}} \quad (1)$$

where $w_{initial}$ is the initial crack width; $w_{after\ sealing}$ is the crack width after sealing.

After re-loading test, the initial crack widths were firstly calculated. Fig. 6 shows the distribution of crack width for samples in different scenarios.

2.4. Ultrasonic pulse velocity test

The UPV test is a widely accepted and commonly used method to evaluate the damage and self-healing performance of concrete [15,32,45,46]. The fundamental working principle of the UPV test is sketched in Fig. 7. It involves the measurement of the velocity of the sound waves that propagate between an emitter and a receiver through the concrete. The velocity of these waves changes when passing through a discontinuity, typically a crack in concrete, as a function of the depth and width of the same crack. For the experiments conducted in this study, the distance between the transmitter and receiver was kept constant at 100 mm. The diameter of the transducer used for the test was 50 mm, and the frequency of the signal used was 50 kHz. The UPV tests were conducted on three types of samples: intact, pre-cracked, and sealed DWES samples after unloading. To calculate the wave velocity, the transmission time of the wave through the sample was recorded. An index of velocity recovery (IVR) was proposed, as shown in Eq. (2), to compare the velocity of the sound waves through the intact, pre-cracked, and sealed samples [42]. Hence, the extent of damage and the effectiveness of the self-healing process can be determined.

$$IVR = \frac{UPV_i}{UPV_{intact}} \quad (2)$$

where UPV_i is the velocity of crack sample in i-th period; UPV_{intact} is the velocity of intact sample.

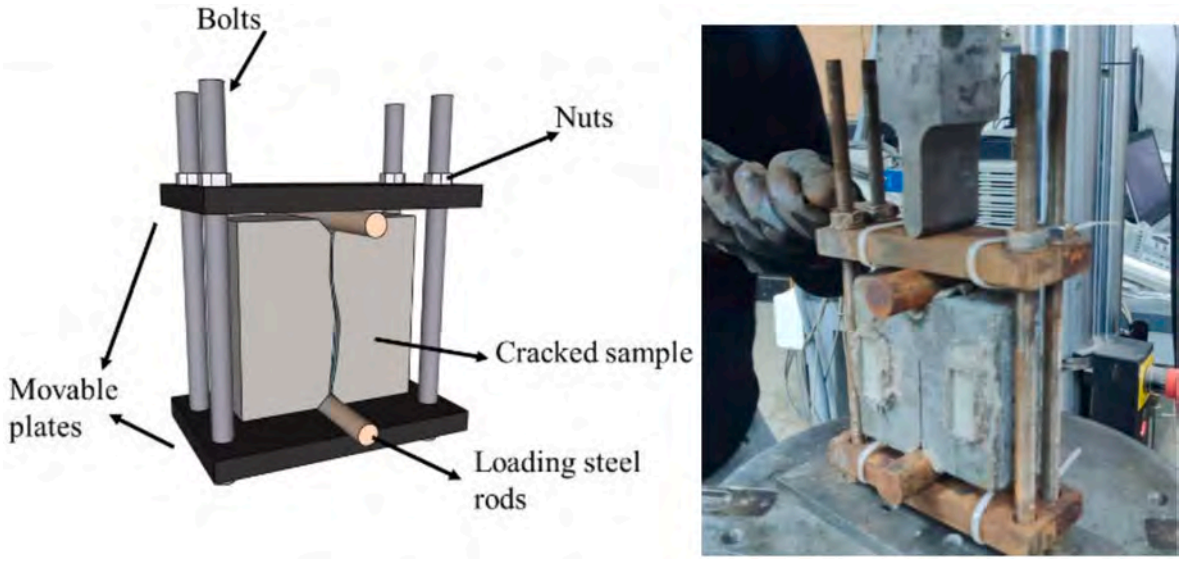

Fig. 3. Set-up for sustained loading DEWS samples.

Table 2
Composition of the geothermal water.

Compositions	Al	Ca	Fe	K	Mg	Na	S	Si	SO_4^{2-}	Cl
Quantity(in ppm)	0.2	4	0.13	19.8	0.3	1243	1523	0.3	2678	441

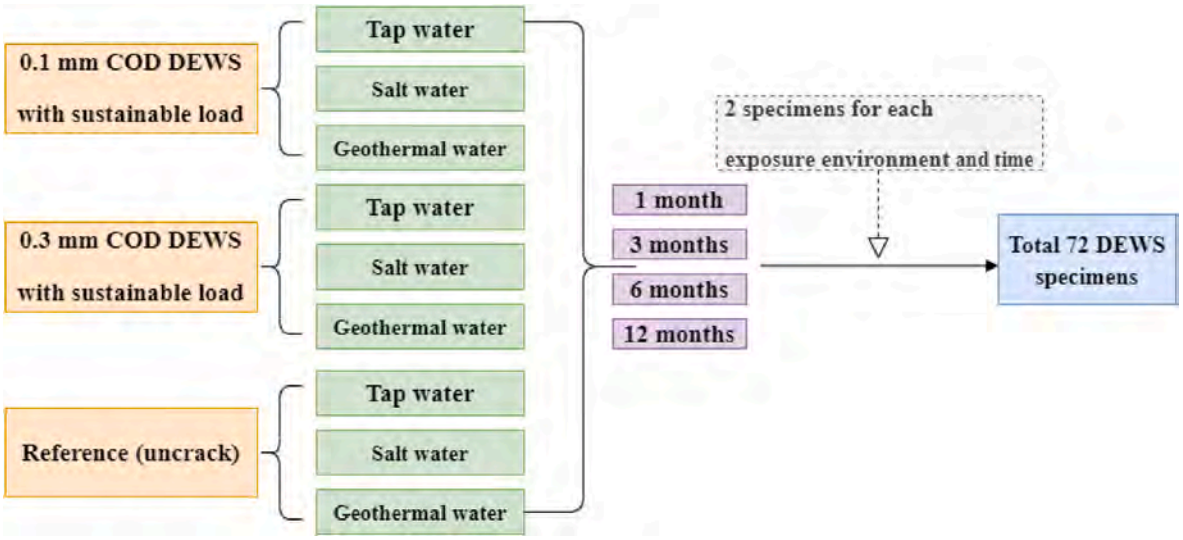

Fig. 4. Test program.

2.5. Final splitting test

To investigate the recovery of mechanical properties of pre-cracked UHPC samples in different exposure environments, the loaded samples were removed from the loading device, after 1,3,6,12 months of exposure, and subjected to a final splitting tensile test. The specimens were loaded at the same rate as in the pre-cracking tests until the samples failed completely. The stress vs. crack open displacement curves were obtained from which an Index of Stiffness Recovery (ISR) was calculated as in Eq. (3) [15,33]. This calculation principle is demonstrated in Fig. 8

$$ISR_0 = \frac{K_c^f - K_u^0}{K_c^0 - K_u^0} \tag{3}$$

where K_c^0 is initial loading stiffness; K_u^0 is unloading stiffness; K_c^f is final loading stiffness after setting exposure time.

2.6. Chloride penetration tests

To evaluate the depth of chloride penetration, samples immersed in saltwater were analyzed, after the final failure tests, with silver nitrate ($AgNO_3$) spraying tests. An $AgNO_3$ solution at 0.1 mol/L concentration was sprayed on the fracture surface of the freshly split DEWS samples. The chloride-free portions took on a light brown color, whereas the chloride-contaminated parts changed to white or light gray [35]. After photographing the titrated regions with optical microscope, the pictures were processed with Photoshop to identify the color change border and

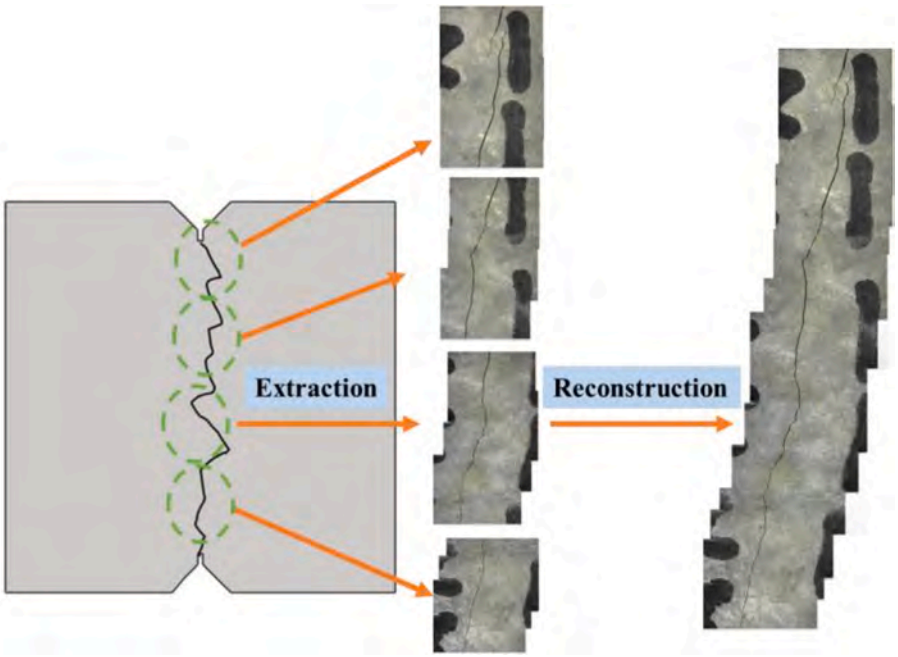

Fig. 5. Schematic of extraction and reconstruction of cracks.

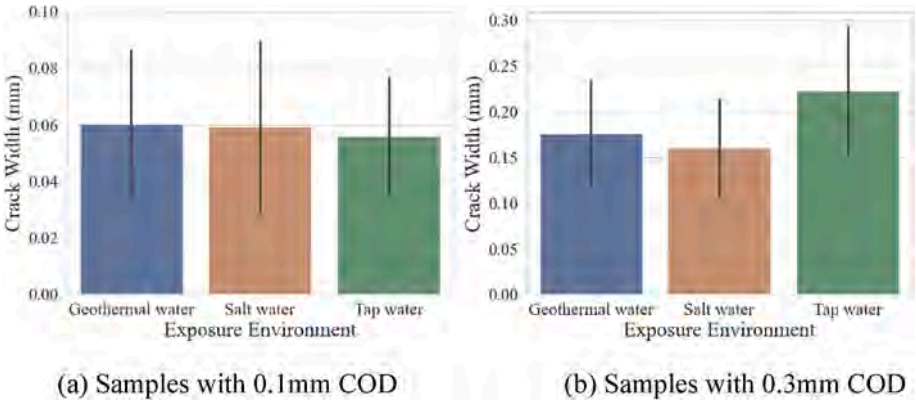

Fig. 6. Distribution of crack width after re-loading test (The error bar is standard deviation).

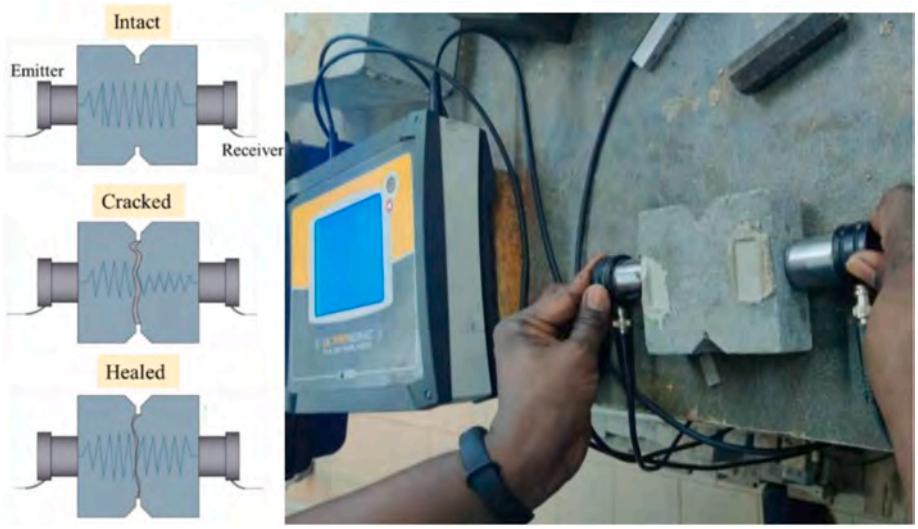

Fig. 7. Schematic diagram of UPV.

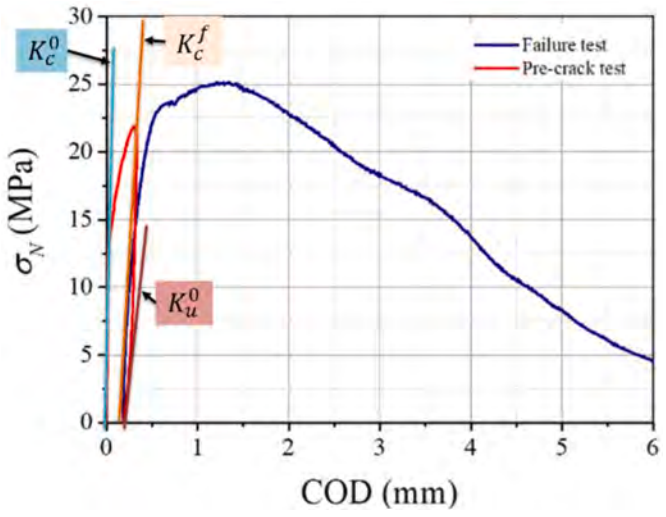

Fig. 8. Definition of the index of stiffness recovery.

calculate the chloride penetration depth.

2.7. SEM

The microstructure and morphological changes of self-healing products in UHPC exposed to various environments, were analyzed using scanning electron microscopy (SEM, ZeissEvo 50P, ZEISS, Oberkochen, Germany). SEM analysis was conducted on the specimens after 3 and 6 months of exposure to different environments. The 10 × 10 × 10 mm test samples were extracted from near the failed DEWS samples after final splitting test. SEM images were obtained in high vacuum mode using an accelerating voltage of 20 kV and a variable working distance. Moreover, energy dispersive X-ray spectroscopy (EDS) analysis was used in conjunction with SEM to determine the major elements distribution in the healing product.

3. Results and discussion

3.1. Index of crack self-sealing

Fig. 9 shows the evolution of cracks width in tap water, salt water, and geothermal water at various exposure times, and Eq. (1) was utilized to compute the ICS, as shown in Fig. 10. The ICS are computed from two samples of the same exposure duration. To observe crack width changes in the early stages, the average ICS from all cracked samples can be examined at both 7 days and 14 days. The crack widths were categorized into narrow ($\leq$ 0.1 mm) and wide (0.1–0.3 mm) ranges. As depicted in Fig. 10, with increasing exposure time, almost all cracks have healed significantly, and better healing outcomes can be achieved with extended healing times. Narrow cracks tend to heal faster and more effectively compared to wider ones. Among the three water environments, samples exposed to tap water exhibited significantly better healing compared to those exposed to salt and geothermal water. In the case of samples with narrow cracks exposed to tap water, rapid crack closure was observed, with the value of ICS reaching 44.6 % after just 7 days, ultimately achieving 100 % closure in only 3 months. Conversely, in salt water, the average value of ICS was 31.3 % after 7 days, and it took 6 months to achieve complete closure. In geothermal water, the value of ICS measured 19.3 % at 7 days, 89 % after 6 months, and even after 12 months of immersion, it reached an average of 97.2 %. Samples with wider crack had an average value of ICS of 98.4 %, 93.9 % and 83.6 % after 6 months exposure to tap water, salt water and geothermal water, respectively. These results suggest that aggressive water environments have a detrimental effect on both the rate and extent of self-healing. It is important to note that, after a 12-month exposure, the ICS values can eventually reach 100 % for samples with wider crack widths exposed to salt water and 85.1 % for those exposed to geothermal water. This indicates that extended exposure periods can overcome the inhibitory impact of aggressive environments on the self-healing potential of UHPC. The effects of aggressive environment on the morphology and nature of self-healing products are going to be discussed further in section 3.5.

3.2. UPV test

The average IVR, represents the extent of healing in the sample under various exposure times and environmental conditions. Fig. 11 shows the initial IVR values varied due to different degrees of sample damage. However, for the same COD group, the initial IVR had a relatively minor impact on the final IVR values. Besides, a gradual increase in the IVR was observed as the exposure time increased. Notably, the samples with 0.1 mm COD showcased a more pronounced rate of as compared to those with 0.3 mm COD. The rate of increase was highest for samples with 0.1 mm COD exposed to tap water, which was one after three months of exposure. This is likely due to water penetration inside the bulk matrix of the specimen which resulted in a broader delayed hydration reaction. Besides, for samples with 0.3 mm COD exposed to tap water, this value reached 0.98 in 6 months and 1 in 12 months. Conversely, samples exposed to saltwater and geothermal water manifested a slower recovery rate, implying a reduced degree of crack closure. The 0.1 mm COD samples exposed to geothermal water displayed a ratio of 0.9 in 3 months, 0.93 in 6 months, and 0.99 in 12 months. This tendency aligns with the ICS analysis. The results emphasize the influence of different exposure environments on the healing rate and level.

3.3. Mechanical properties recovery

The calculations of ISR for all the tested samples were performed based on Eq. (2) and Fig. 8, for different environments and exposure time. Fig. 12 shows that after one month, all the samples under sustained loads displayed varying degrees of stiffness recovery, indicating that the cracks were not only sealed but healed as well, thus enabling the cracked UHPC to recover its mechanical properties owing to the effect of self-healing. Moreover, Fig. 12 (a) shows the ISR values of the 0.1 mm COD samples were found to be higher than that of the 0.3 mm COD samples. For example, after 3 months, the 0.1 mm COD samples were observed to have an ISR of 27.7 % upon exposure to tap water, whereas the 0.3 mm COD samples in Fig. 12 (b) had an ISR of 21 %.

The results of ICS and UPV signify that smaller cracks lead to higher levels of self-healing. Furthermore, the mechanical recovery ability depends on the degree of sample damage. The same ICS values were obtained after up to 12 months, and samples with COD of 0.3 mm present lower ISR values than samples with a COD of 0.1 mm for same exposure conditions. This indicates that the higher degree of damage makes the mechanical property recovery more difficult. For comparison sake, it is worth citing a study by Lo Monte and Ferrara [33] who revealed that the pre-cracked beam, XA-CA, recovered over 60 % of its stiffness after being continuously exposed to geothermal water for one month, and almost reached 100 % recovery after 6 months. The primary reason for this difference in stiffness recovery was the formation of multiple cracks with widths less than 0.05 mm during the bending tests of the beams. As discussed earlier, narrower cracks are more likely to recover their strength. In contrast, the DEWS samples typically formed only 1–2 wider cracks after pre-cracking, which largely prevented residual crack width recovery under load.

The recovery of mechanical properties was shown to be higher in samples exposed to tap water than others. Specifically, the ISR of the 0.1 mm COD samples were observed to be 16.6 %, 15.4 %, and 12.5 % upon exposure to tap water, salt water, and geothermal water, respectively, after one month of exposure. Similarly, after 6 months, the ISR values

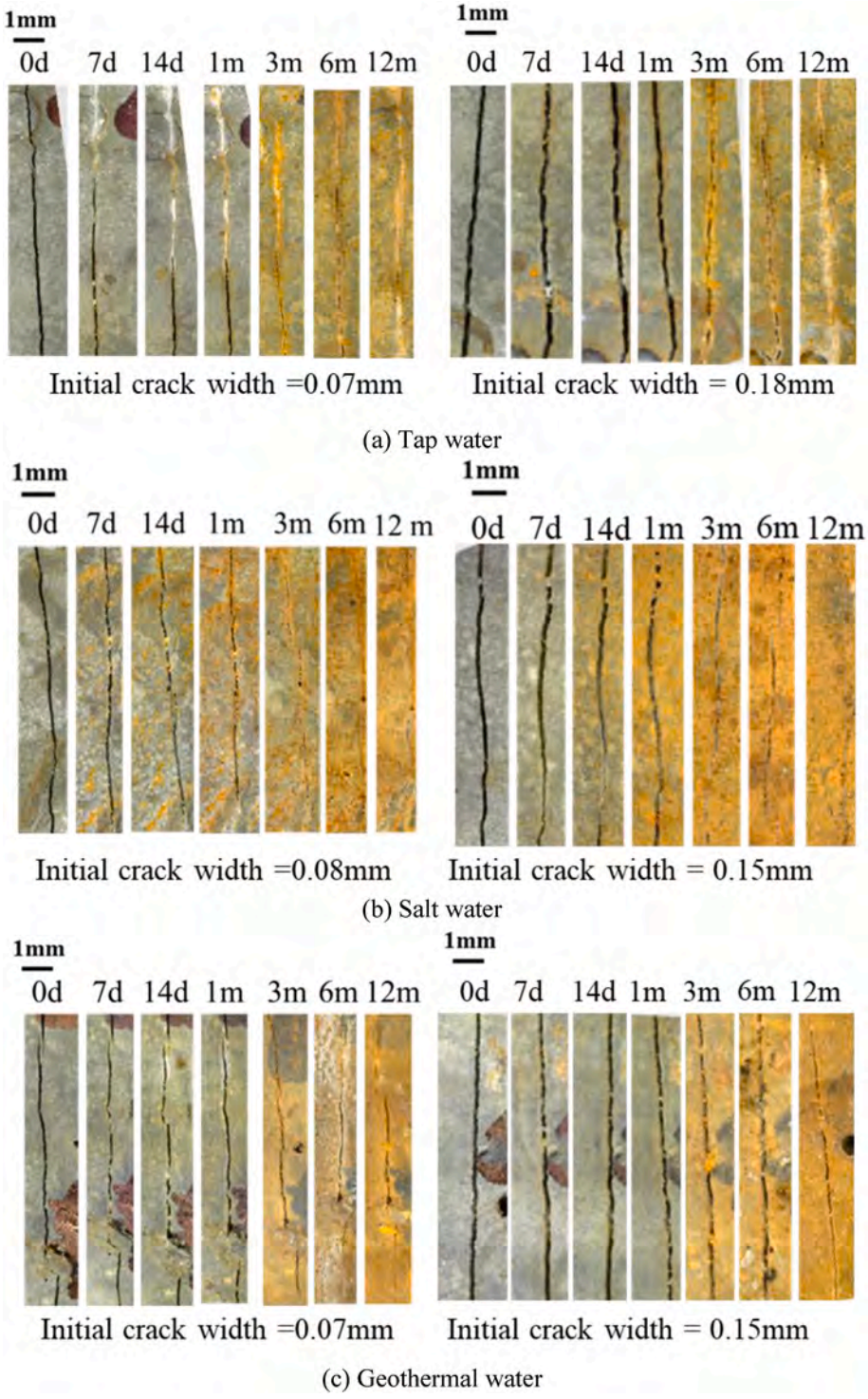

Fig. 9. Variation of crack width in different environments and times.

were 30.1 %, 29.6 %, and 24.9 %, respectively. However, after 12 months exposure, the difference in ISR between samples with 0.1 mm COD was minimal, where it was 39.1 % in tap water, 38.8 % in salt water, and 36.1 % in geothermal water. Notably, some studies reveal that the recovery of mechanical properties can be improved by the effect of chloride ions [47–49]. That may be due to the generation of Friedel's salt through the reaction of chloride ions with hydration products in concrete and/or an increase in roughness from mild corrosion of steel fibres, which may increase the friction between the fibres and the matrix [47,49–51].

Moreover, although ISR growth was promoted by prolonged exposure, the ISR rising rate decelerated over time. For example, the rate for samples exposed to 0.1 mm COD in tap water was 16.5 %, 9.2 %, 5 %, and 3.9 % per month for the 1st, 3rd, 6th, and 12th months, respectively. The reasons can be attributed to two main factors. Firstly, there is a reduction in active reactive substances within the concrete. Secondly, the self-healing process itself promotes further closure of the cracks, impeding the entry of external water required for healing. Previous studies have emphasized that when previously healed fractured concrete samples experience further cracking and undergo healing again after a

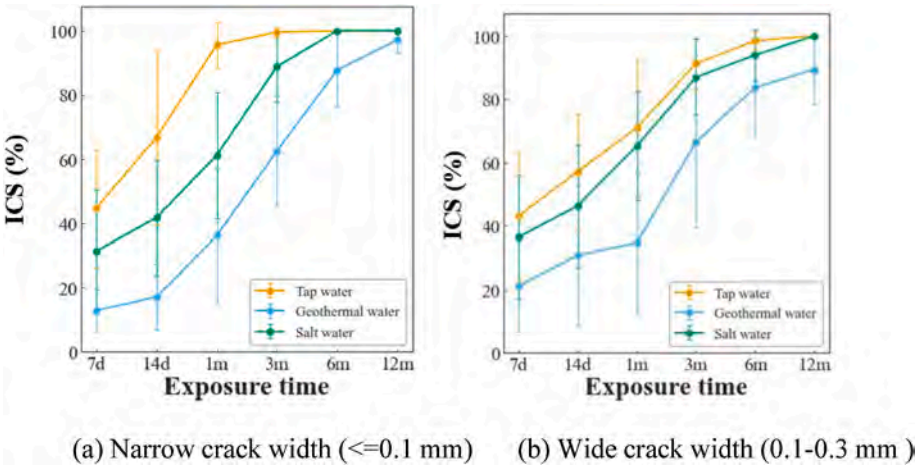

Fig. 10. Comparison of ICS (The error bar is standard deviation).

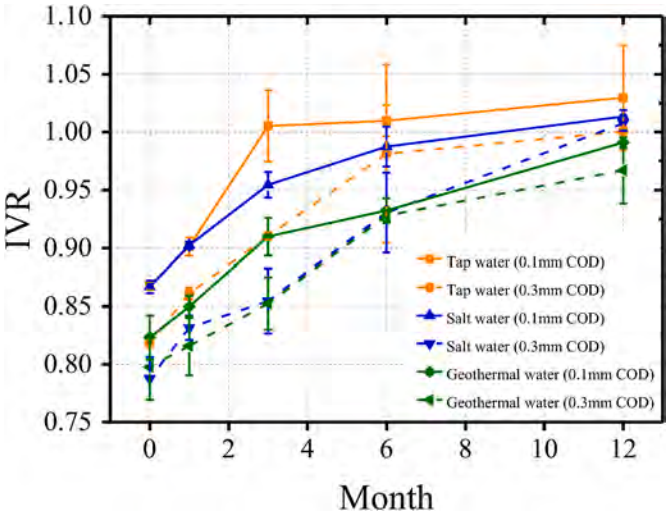

Fig. 11. IVR from UPV tests (The error bar is standard deviation).

certain period, the mechanical recovery of the concrete can be further enhanced. This is because the further opening of cracks allows water to penetrate the interior of the concrete once more [44,52]. It is vital to recognize that despite exposure to salt water and geothermal water, no degradation in the mechanical properties of cracked UHPC with sustained load was observed. This may be owing to UHPC's high self-healing property and impermeability.

The mechanical properties of DEWS were evaluated according to the post-exposure splitting test. Fig. 13 summarizes the variation of the peak stresses and Fig. 14 shows the evolution of the average stress-COD curve. This peak stress is highly variable. It is mainly controlled by the distribution and orientation of the fibres [41]. But the peak stresses did not differ significantly from those of the reference samples even when pre-cracking was subjected to sustainable loading and aggressive conditions, and no significant tensile stiffness degradation was observed, indicating that the material is highly durable and resilient.

3.4. $AgNO_3$ solution spray test

Fig. 15 compares the results of the AgNO3 solution spray test for samples exposed to salt water with a concentration of 3.3 g/L at different exposure times. It was found that the wider the crack width and the longer the exposure time, the higher the depth of chloride ion penetration inside the UHPC. Fig. 16 further shows the average penetration velocity of chloride ions and compares the differences in crack closure levels for different samples. Although wider cracks resulted in higher chloride ion penetration velocities, the penetration velocity decreased significantly with increasing exposure time. This is mainly attributed to the fact that the cracks close under the influence of self-healing, thus preventing further chloride ion penetration. At the sample with 0.1 mm COD, the chloride ion penetration rate was 0.934 mm/month after one month of exposure to salt water, with a corresponding ICS value of 64.6 %. After 6 months and 12 months, the penetration velocity decreased by 36.4 % to 0.594 mm/month and by 55.5 % to 0.425 mm/month, and

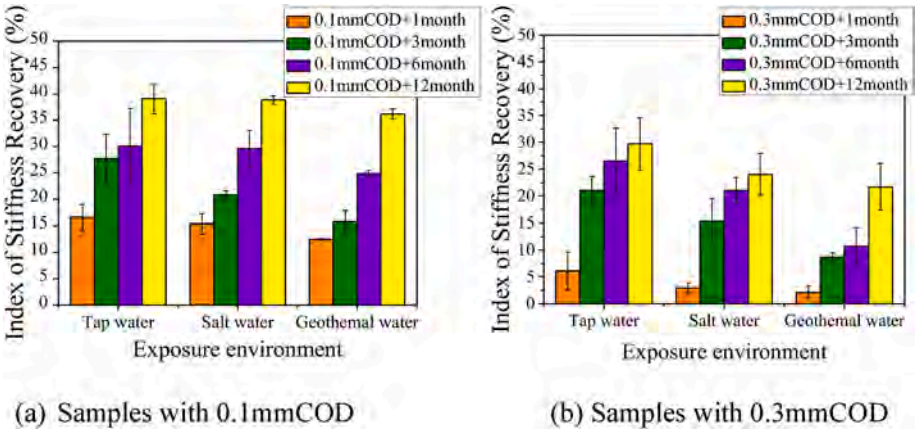

Fig. 12. Comparison of ISR (The error bar is standard deviation).

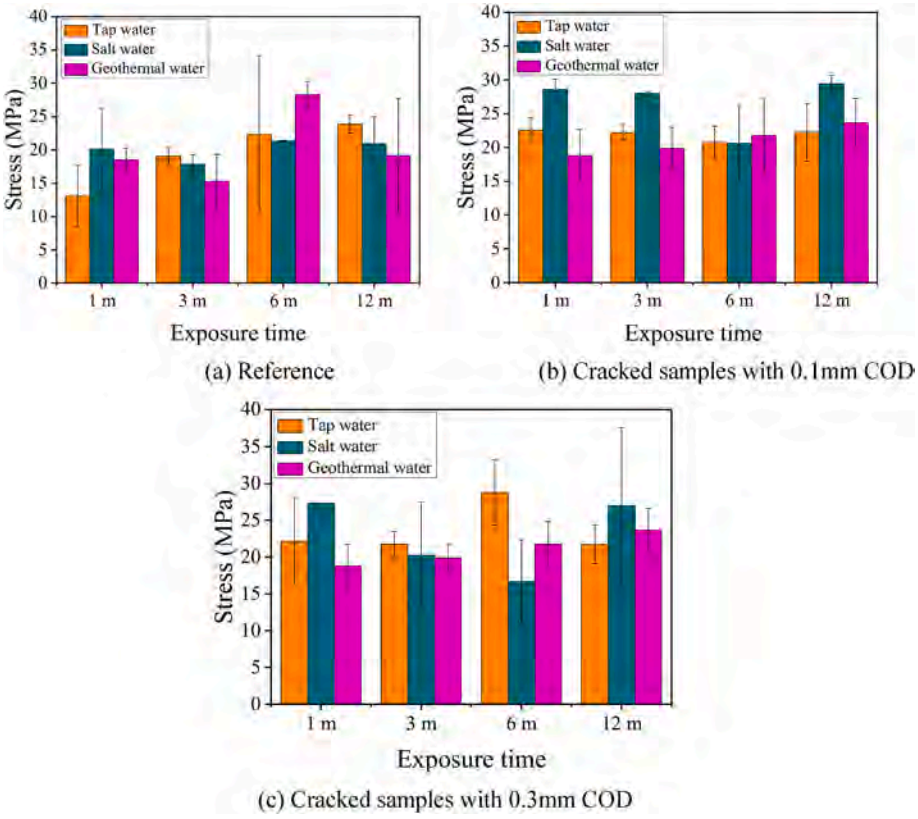

Fig. 13. Evolution of peak stress recorded by final splitting test (The error bar is standard deviation).

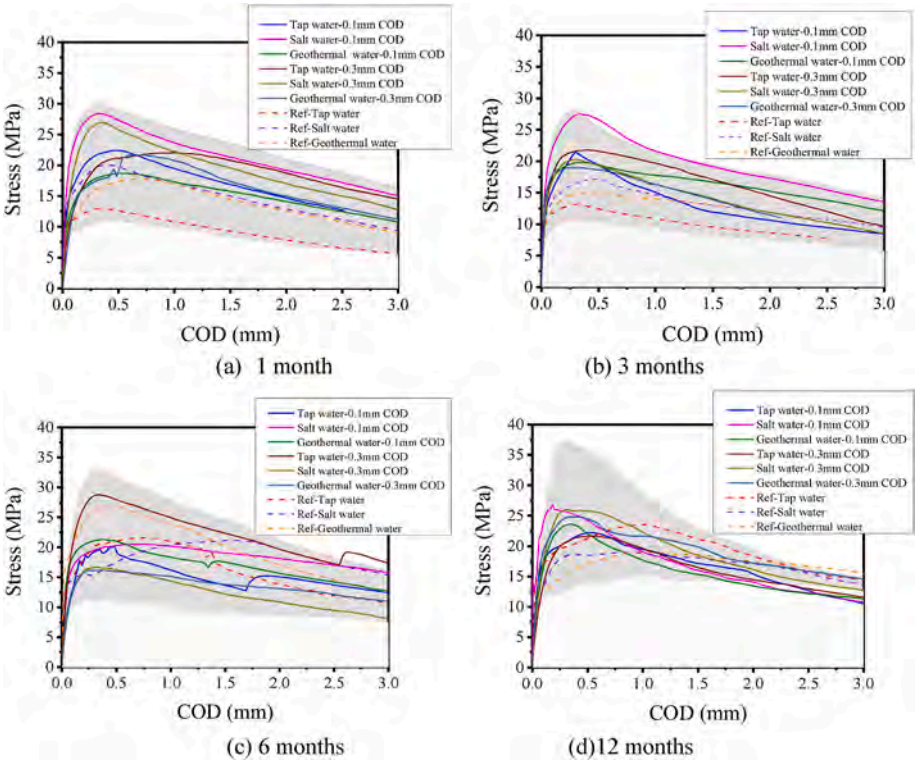

Fig. 14. Average stress-COD curves.

their corresponding ICS values were 100 %. In addition, the difference in chloride ion permeation velocity between the wide and narrow cracks in the samples gradually decreased with increasing exposure time. At one month, the average chloride ion permeation velocity of the sample with COD of 0.3 mm was 2.25 times higher than that of the sample with COD of 0.1 mm. After 3 months, this ratio was 1.43, a decrease of 36.6 %, and

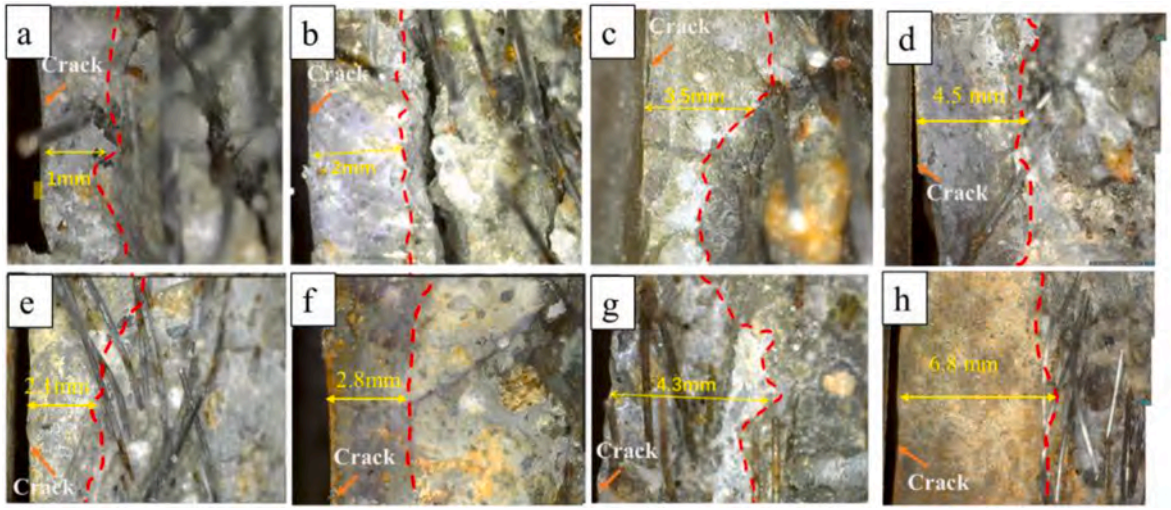

Fig. 15. Comparison of depth of chloride penetration. (a) Sample with 0.1 mm COD in one month; (b) sample with 0.1 mm COD in 3 months; (c) sample with 0.1 mm COD in 6 months; (d) sample with 0.1 mm COD in 12 months; (e) sample with 0.3 mm COD in one month; (f) samples with 0.3 mm COD in 3 months; (g) sample with 0.3 mm COD in 6 months; (h) sample with 0.3 mm COD in 12 months.

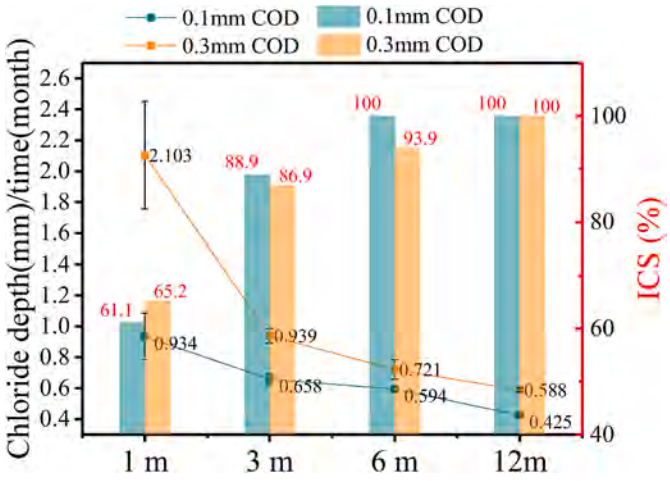

Fig. 16. Relationship between chloride penetration velocity and ICS. ICS – 0.1 and 0.3 mm COD for the histograms and Chloride depth/time – 0.1 and 0.3 mm COD.

after 12 months, the ratio was 1.38, a decrease of 38.5 %. Longer exposure times also allowed 100 % ICS values to be obtained even for wider cracks and improve chloride resistance.

3.5. *Morphology of self-healing products and distribution of elements in cracks*

Fig. 17 shows that after the samples were exposed to tap water for 3 months, some self-healing products were found attached to the fibre surface, which were confirmed by EDS analysis to consist mainly of carbon (C), oxygen (O), and calcium (Ca) elements. Previous studies have also shown that the main component of the self-healing products is $CaCO_3$ [35,53,54]. Additionally, the morphology of the products observed on the fibre surface exhibited a polyhedral structure, which is a characteristic feature of calcite - the most stable crystalline form of $CaCO_3$ [55–57]. Upon further exposure of the samples to tap water for 6 months, the fibre surface was found to be covered with numerous fragments of the matrix (Fig. 18). The fibres can act as deposition site for the healing products and this also results into a growth of the products along the fibre matrix interface which is beneficial to healing. The self-healing products possibly strengthen the bond between the fibre and matrix [58], leading to increased matrix detachment.

After exposure of the samples to salt water for 3 months, EDS area map analysis was conducted, and Fig. 19 illustrates the major elements' distribution in the matrix on the fracture surface. The image brightness indicated the concentration of chemical elements, with the brightest areas representing the highest element content. The analysis revealed that Cl^- and Na^+ elements were present in the matrix on the crack surface, mainly distributed at the interface between the steel fibres and the matrix. This indicates that chloride ions infiltrated the interior of the UHPC along the cracks and further reached the interface between the UHPC matrix and the steel fibres. Additionally, EDS analysis showed that the self-healing products were also $CaCO_3$, but their morphology did not exhibit a clear polyhedral structure (Fig. 20). Qian et al. suggested that NaCl can slow down the crystallization of $CaCO_3$ and reduces its thermodynamic and kinetic potential [59]. Moreover, NaCl hinders the growth of the (1 0 4) and (1 1 0) facets of calcite [59]. However, with prolonged exposure of the samples to salt water for 6 months, the fibre surfaces were also found to be covered with many matrix fragments, indicating a possible improvement in the bond at the fibre-matrix interface level (Fig. 21).

For samples exposed to geothermal water, after 3 months, EDS mapping scanning results showed the distribution of sulfur (blue part) (Fig. 22). This is due to the high amount of sulfate ions contained in the geothermal water. For the fiber, it was observed that the surface of the fibers was very smooth and not many crystal particles were found covering it (Fig. 23). The sulfate was also able to reduce the precipitation rate of $CaCO_3$ [60,61]. In geothermal water, the crystallization of $CaCO_3$ may be hindered by the dual action of sulfate and chloride ions. After 6 months of exposure, some polyhedral $CaCO_3$ particles were also found on the surface of the fibers (Fig. 24).

The results from SEM and EDS revealed that the self-healing products, whose main elements were detected as calcium carbon and oxygen almost irrespective of the exposure conditions, were mainly $CaCO_3$, despite the exposure of the samples to different environments. When the samples were exposed to tap water, more polyhedral $CaCO_3$ crystals could be found, indicating a higher crystallinity of the crystals. In contrast, when the samples were exposed to salt water and geothermal water, the crystallization rate of $CaCO_3$ may have been reduced due to the influence of the chloride and/or sulfate ions. This also explains why exposure to tap water has a higher level of self-healing performance recovery than on exposure to others. Nonetheless, the prolonged exposure and the continuous progress of the healing was able to counteract

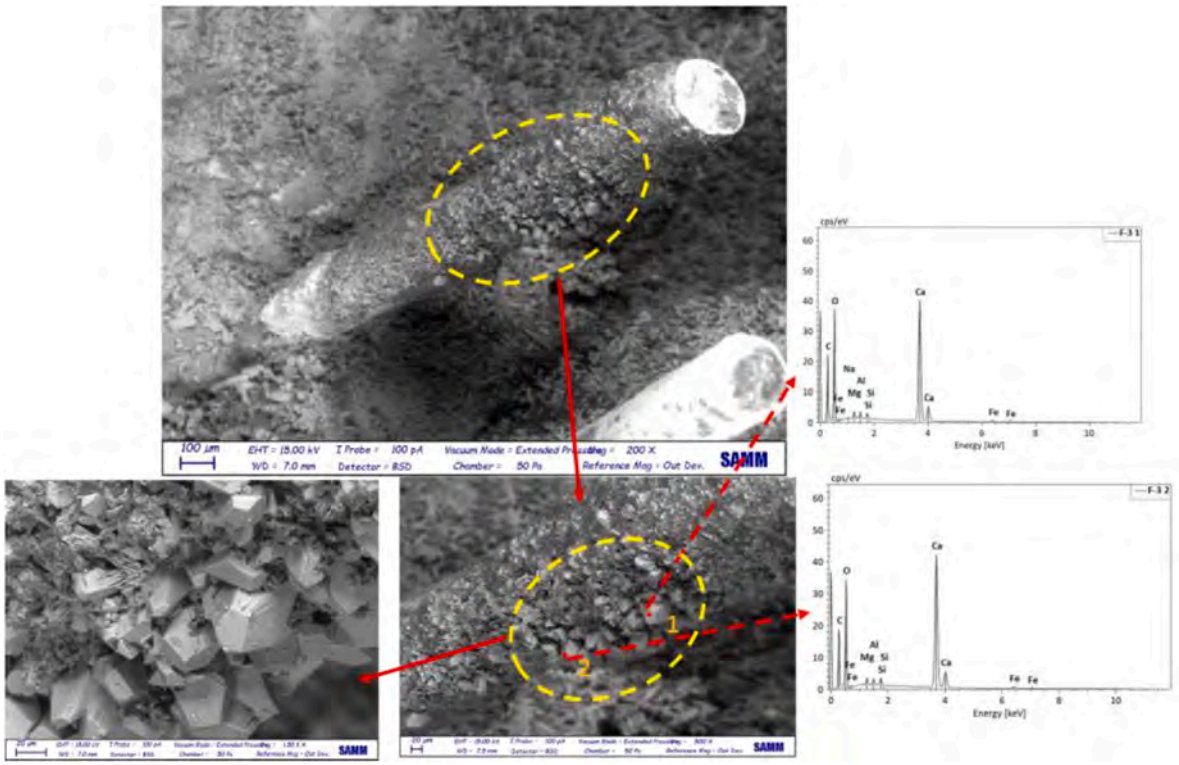

Fig. 17. The images of SEM and EDS for the samples exposed to tap water in three months.

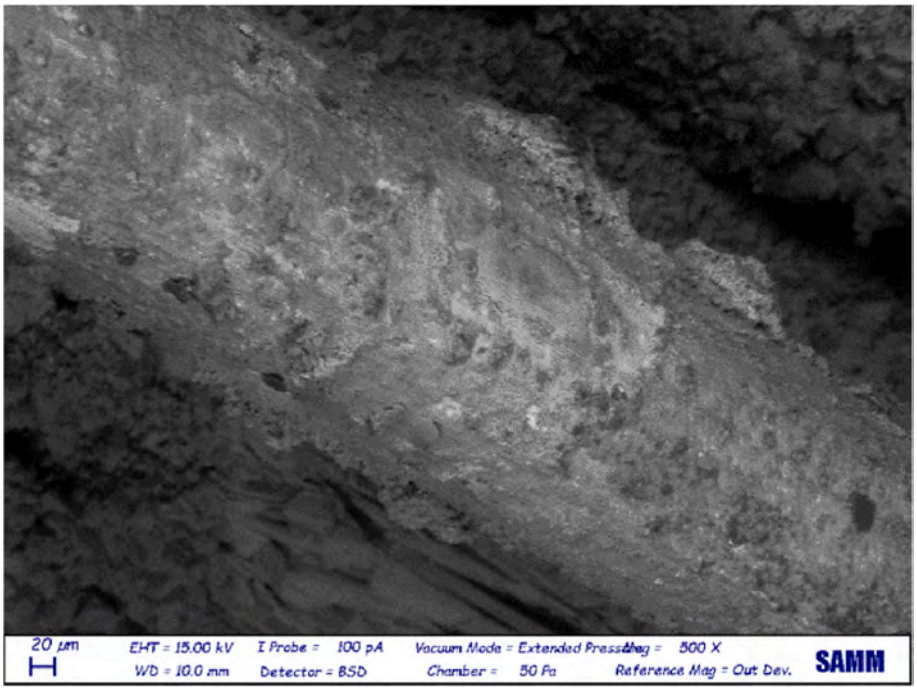

Fig. 18. The fibre SEM image for the samples exposed to tap water in six months.

the possible lowering effects due to the aggressiveness of the exposure environment, even under sustained through crack tensile stress which is not favourable to crack healing.

4. Conclusions

This study examined the self-healing capabilities of UHPC under contemporary environmental and sustained mechanical conditions. The authors designed and constructed a sustained load setup to validate the impact of continuous tensile stresses and environmental exposure on UHPC through cracks. Various test methods and evaluation indices were employed to assess the evolution of UHPC's self-healing performance. The following conclusions can be drawn from this investigation:

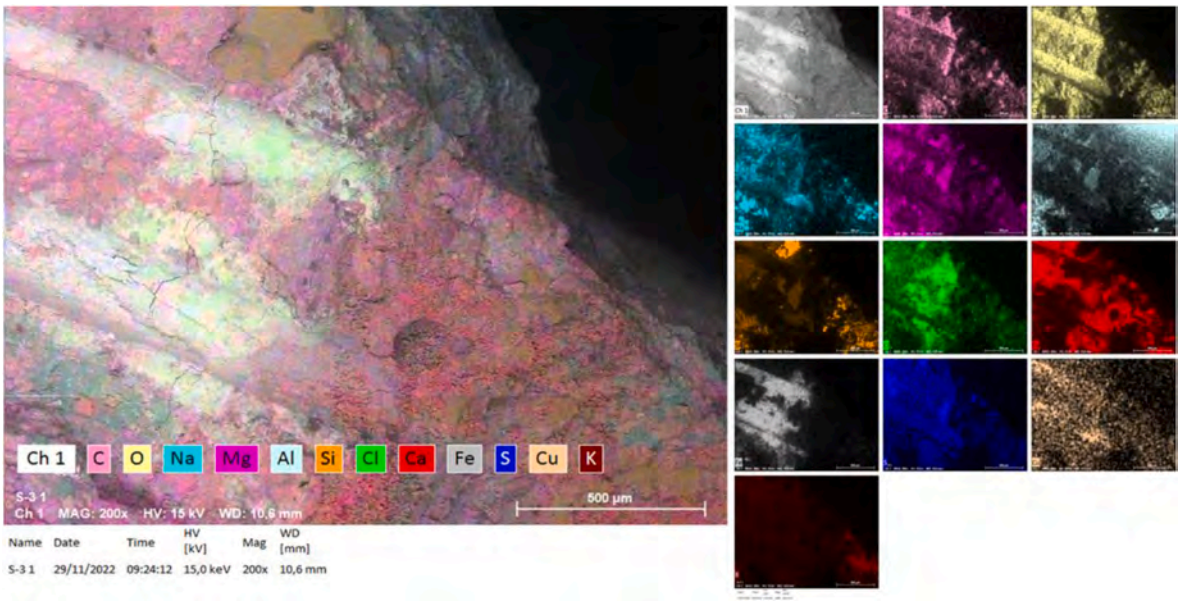

Fig. 19. EDS elemental maps images for the sample exposed to salt water in three months.

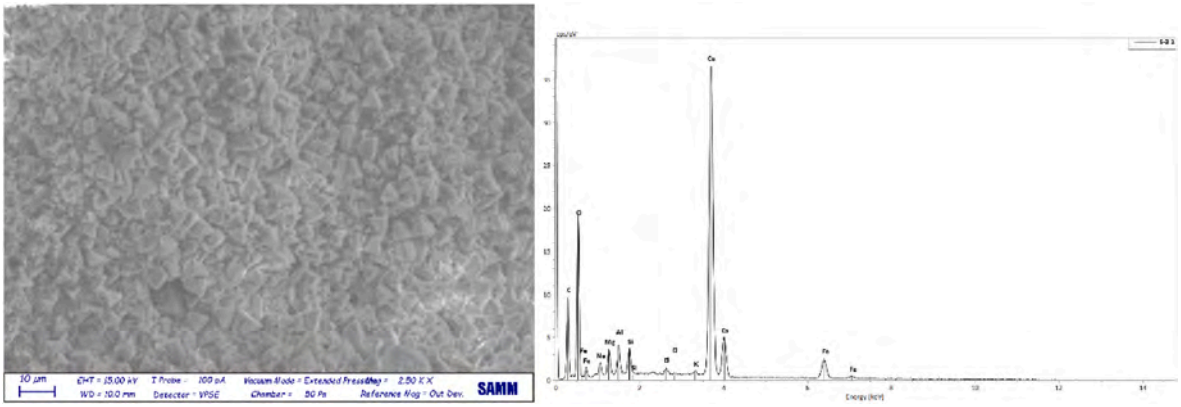

Fig. 20. The self-healing product SEM and EDS images for the sample exposed to salt water in three months.

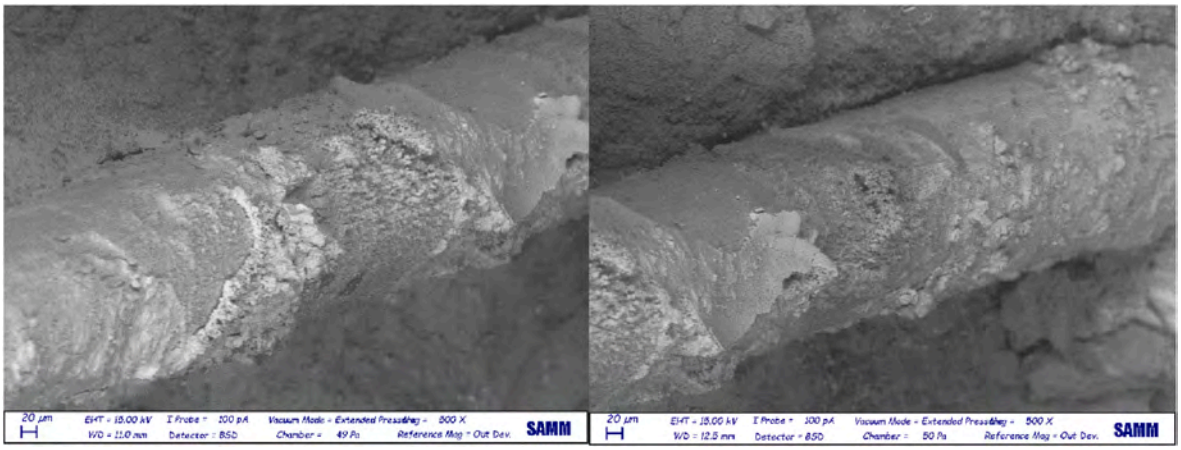

Fig. 21. The observation of steel fiber for the sample exposed to salt water in six months.

1 With longer exposure, self-healing level improves significantly. Samples in tap water exhibit exceptional healing performance compared to saltwater and geothermal water. Narrow cracks immersed in tap water close rapidly, achieving complete closure (100 % ICS) in just 3 months. In saltwater, the average ICS reaches 100 % after 6 months, while in geothermal water, it reaches 89 % in the same period. Aggressive environments noticeably affect self-healing rates and levels. For wider cracks, extended exposure (12

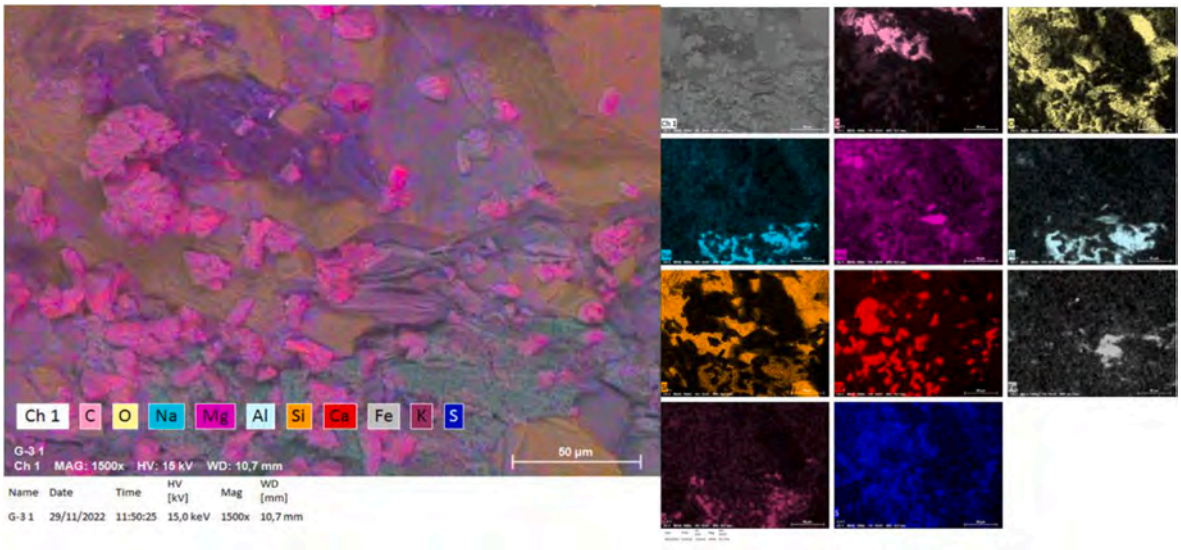

Fig. 22. EDS elemental map images for the sample exposed to geothermal water in three months.

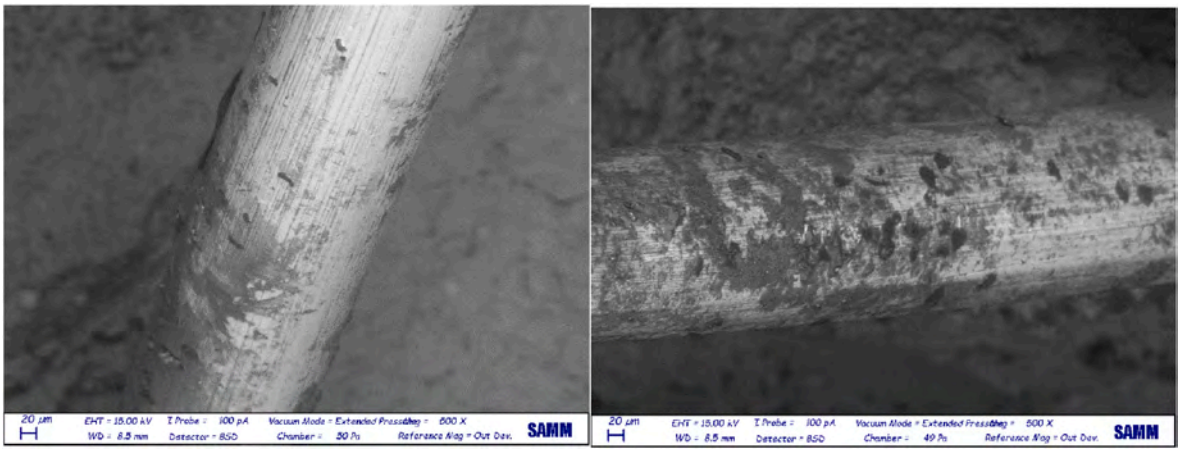

Fig. 23. The observation of steel fibre for the sample exposed to geothermal water in six months.

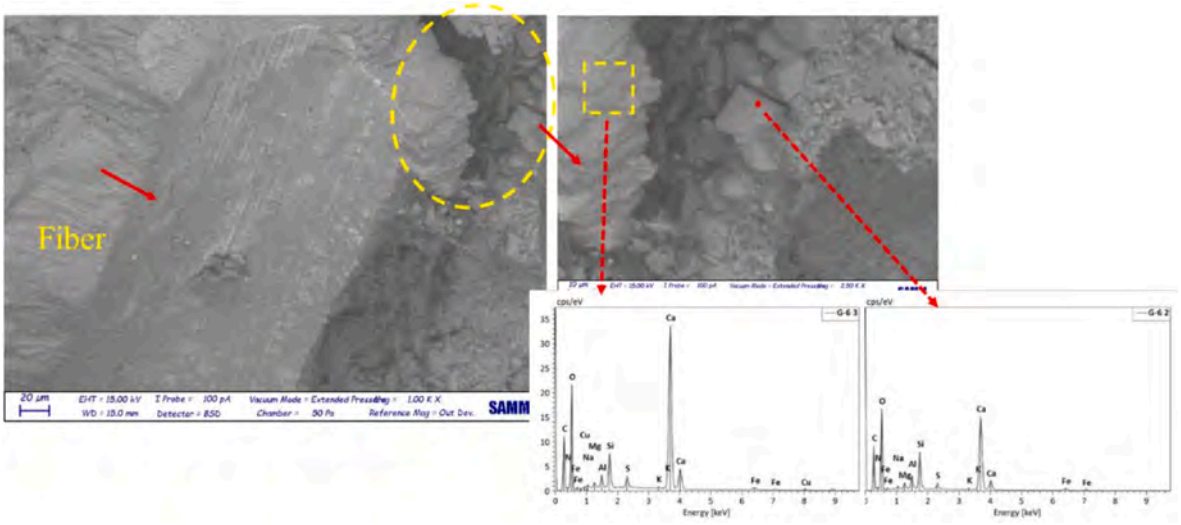

Fig. 24. The self-healing product SEM and EDS images for the sample exposed to geothermal water in six months.

months) in saltwater and geothermal water allows ICS to reach 100 % and 85.1 %, respectively, overcoming the inhibitory effects of aggressive conditions on self-healing.

2 The IVR increased gradually over time. However, specimens in geothermal and saltwater showed slower recovery rates, indicating limited crack restoration. These results are consistent with the ICS analysis.

3 The increase in ISR values indicates stiffness recovery despite sustained loading. The self-healing effect enables the cracked UHPC to regain its mechanical properties, resulting in an overall stiffness improvement of 20–40 % after 12 months. Samples with 0.1 mm COD exhibited higher ISR values compared to those with 0.3 mm COD. Samples exposed to tap water exhibited better mechanical property recovery than those exposed to saltwater and geothermal water. After 12 months, the ISR difference between samples with 0.1 mm COD was minimal, and while prolonged exposure continued to boost ISR, the rate of increase gradually declined.

4 The $AgNO_3$ solution spray test revealed that wider cracks and longer exposure times led to deeper chloride ion penetration. Nevertheless, the rate of penetration significantly decreased as exposure time increased. This reduction primarily occurred because the cracks sealed themselves through self-healing, preventing further chloride ion penetration.

5 SEM and EDS results revealed that the self-healing products in the samples primarily consisted of $CaCO_3$, regardless of the environment. In tap water, there were more polyhedral calcite-characterized $CaCO_3$ crystals on fibre surface, indicating higher crystallinity. Upon exposure to salt and geothermal water for 3 months, the $CaCO_3$ crystallization rate declined due to chloride and/or sulfate ions' influence. However, even after 6 months of exposure, numerous polyhedral $CaCO_3$ crystals were still present. The prolonged exposure and continuous healing process counteracted potential reductions caused by the aggressive exposure environment.

Declaration of competing interest

The authors declare that they have no known competing financial interests or personal relationships that could have appeared to influence the work reported in this paper.

Data availability

Data will be made available on request.

Acknowledgements

The research activity reported in this paper has been performed in the framework of the ReSHEALience project (Rethinking coastal defense and Green-energy Service infrastructures through enHancEd-durAbiLity high-performance cement-based materials) which has received funding from the European Union's Horizon 2020 research and innovation program under grant agreement No 760824. The help of Mr. Antonio Cocco, Mr. Paolo Broglia and Mr. Giuseppe Pappadà (Laboratory for Testing Materials, Buildings and Structures, Politecnico di Milano) in cutting the specimens for the experimental program and providing organizational support for its execution is gratefully acknowledged. Bin Xi and Zhewen Huang also acknowledge the financial support of the China Scholarship Council (CSC) under the grant No.202008440524 and No.202207820024 for PhD studies in Structural Geotechnical and Earthquake Engineering at Politecnico di Milano.

References

[1] H. Van Damme, Concrete material science: past, present, and future innovations, Cement Concr. Res. 112 (2018) 5–24, https://doi.org/10.1016/j.cemconres.2018.05.002.

[2] A. Neville, Consideration of durability of concrete structures: past, present, and future, Mater. Struct. (2001), https://doi.org/10.1007/bf02481560.

[3] H. Beushausen, R. Torrent, M.G. Alexander, Performance-based approaches for concrete durability: state of the art and future research needs, Cement Concr. Res. 119 (2019) 11–20, https://doi.org/10.1016/j.cemconres.2019.01.003.

[4] S. Al-Obaidi, P. Bamonte, F. Animato, F. Lo Monte, I. Mazzantini, M. Luchini, S. Scalari, L. Ferrara, Innovative design concept of cooling water tanks/basins in geothermal power plants using ultra-high-performance fiber-reinforced concrete with enhanced durability, Sustainability 13 (2021) 9826, https://doi.org/10.3390/su13179826.

[5] G. Culivicchi, C.G. Palmerini, V. Scolari, Behaviour of materials in geothermal environments, Geothermics (1985), https://doi.org/10.1016/0375-6505(85)90095-1.

[6] A. Manzella, R. Bonciani, A. Allansdottir, S. Botteghi, A. Donato, S. Giamberini, A. Lenzi, M. Paci, A. Pellizzone, D. Scrocca, Environmental and social aspects of geothermal energy in Italy, Geothermics (2018), https://doi.org/10.1016/j.geothermics.2017.11.015.

[7] A.M. Tahwia, G.M. Elgendy, M. Amin, Durability and microstructure of eco-efficient ultra-high-performance concrete, Construct. Build. Mater. 303 (2021), 124491, https://doi.org/10.1016/j.conbuildmat.2021.124491.

[8] O.R. Abuodeh, J.A. Abdalla, R.A. Hawileh, Assessment of compressive strength of Ultra-high Performance Concrete using deep machine learning techniques, Appl. Soft Comput. J. 95 (2020), 106552, https://doi.org/10.1016/j.asoc.2020.106552.

[9] B. Xi, Z. Huang, S. Al-Obaidi, L. Ferrara, Predicting ultra high-performance concrete self-healing performance using hybrid models based on metaheuristic optimization techniques, Construct. Build. Mater. 381 (2023), 131261, https://doi.org/10.1016/j.conbuildmat.2023.131261.

[10] N.P. Kannikachalam, D. di Summa, R.P. Borg, E. Cuenca, M. Parpanesi, N. De Belie, L. Ferrara, Assessment of sustainability and self-healing performances of recycled ultra-high-performance concrete, ACI Mater. J. 120 (2023), https://doi.org/10.14359/51737336.

[11] ACI Committee 239, Ultra-high-performance concrete: an emerging technology report (ACI 239r–18), Am. Concr. Inst. (2018).

[12] I.L. Larsen, R.T. Thorstensen, The influence of steel fibres on compressive and tensile strength of ultra high performance concrete: a review, Construct. Build. Mater. 256 (2020), 119459, https://doi.org/10.1016/j.conbuildmat.2020.119459.

[13] Z. Zhou, P. Qiao, Direct tension test for characterization of tensile behavior of ultra-high performance concrete, J. Test. Eval. 48 (2020), 20170644, https://doi.org/10.1520/JTE20170644.

[14] L. Teng, H. Huang, K.H. Khayat, X. Gao, Simplified analytical model to assess key factors influenced by fiber alignment and their effect on tensile performance of UHPC, Cem. Concr. Compos. 127 (2022), 104395, https://doi.org/10.1016/j.cemconcomp.2021.104395.

[15] M. Davolio, S. Al-Obaidi, M.Y. Altomare, F. Lo Monte, L. Ferrara, A methodology to assess the evolution of mechanical performance of UHPC as affected by autogenous healing under sustained loadings and aggressive exposure conditions, Cem. Concr. Compos. 139 (2023), 105058, https://doi.org/10.1016/j.cemconcomp.2023.105058.

[16] C. Shi, Z. Wu, J. Xiao, D. Wang, Z. Huang, Z. Fang, A review on ultra high performance concrete: Part I. Raw materials and mixture design, Construct. Build. Mater. 101 (2015) 741–751, https://doi.org/10.1016/j.conbuildmat.2015.10.088.

[17] R. Yu, P. Spiesz, H.J.H. Brouwers, Development of an eco-friendly Ultra-High Performance Concrete (UHPC) with efficient cement and mineral admixtures uses, Cem. Concr. Compos. 55 (2015) 383–394, https://doi.org/10.1016/j.cemconcomp.2014.09.024.

[18] S. Al-Obaidi, M. Davolio, F. Lo Monte, F. Costanzi, M. Luchini, P. Bamonte, L. Ferrara, Structural validation of geothermal water basins constructed with durability enhanced ultra high performance fiber reinforced concrete (Ultra High Durability Concrete), Case Stud. Constr. Mater. 17 (2022), e01202, https://doi.org/10.1016/j.cscm.2022.e01202.

[19] B. Xi, Z. Huang, S. Al-Obaidi, F. Lo Monte, L. Ferrara, Investigation of self-healing property of UHPC with sustained loads under aggressive exposure environments, Fib Symp (2022) 329–336.

[20] N.P. Kannikachalam, P.S. Marin Peralta, D. Snoeck, N. De Belie, L. Ferrara, Assessment of impact resistance recovery in Ultra High-Performance Concrete through stimulated autogenous self-healing in various healing environments, Cem. Concr. Compos. 143 (2023), 105239, https://doi.org/10.1016/j.cemconcomp.2023.105239.

[21] M. Amran, S.S. Huang, A.M. Onaizi, N. Makul, H.S. Abdelgader, T. Ozbakkaloglu, Recent trends in ultra-high performance concrete (UHPC): current status, challenges, and future prospects, Construct. Build. Mater. (2022), https://doi.org/10.1016/j.conbuildmat.2022.129029.

[22] J. Du, W. Meng, K.H. Khayat, Y. Bao, P. Guo, Z. Lyu, A. Abu-obeidah, H. Nassif, H. Wang, New development of ultra-high-performance concrete (UHPC), Composites, Part B 224 (2021), 109220, https://doi.org/10.1016/j.compositesb.2021.109220.

[23] Z. Zhou, P. Qiao, Durability of ultra-high performance concrete in tension under cold weather conditions, Cem. Concr. Compos. 94 (2018) 94–106, https://doi.org/10.1016/j.cemconcomp.2018.08.019.

[24] Z. Ma, T. Zhao, X. Yao, Influence of applied loads on the permeability behavior of ultra high performance concrete with steel fibers, J. Adv. Concr. Technol. 14 (2016) 770–781, https://doi.org/10.3151/jact.14.770.

[25] S. Kim, D.-Y. Yoo, M.-J. Kim, N. Banthia, Self-healing capability of ultra-high-performance fiber-reinforced concrete after exposure to cryogenic temperature, Cem. Concr. Compos. 104 (2019), 103335, https://doi.org/10.1016/j.cemconcomp.2019.103335.

[26] J.L. García Calvo, G. Pérez, P. Carballosa, E. Erkizia, J.J. Gaitero, A. Guerrero, Development of ultra-high performance concretes with self-healing micro/nano-additions, Construct. Build. Mater. 138 (2017) 306–315, https://doi.org/10.1016/j.conbuildmat.2017.02.015.
[27] B. Xi, S. Al-Obaidi, L. Ferrara, Effect of different environments on the self-healing performance of Ultra High-Performance Concrete – a systematic literature review, Construct. Build. Mater. 374 (2023), 130946, https://doi.org/10.1016/j.conbuildmat.2023.130946.
[28] E. Cuenca, V. Postolachi, L. Ferrara, Cellulose nanofibers to improve the mechanical and durability performance of self-healing Ultra-High Performance Concretes exposed to aggressive waters, Construct. Build. Mater. 374 (2023), 130785, https://doi.org/10.1016/j.conbuildmat.2023.130785.
[29] V. Cappellesso, D. di Summa, P. Pourhaji, N. Prabhu Kannikachalam, K. Dabral, L. Ferrara, M. Cruz Alonso, E. Camacho, E. Gruyaert, N. De Belie, A review of the efficiency of self-healing concrete technologies for durable and sustainable concrete under realistic conditions, Int. Mater. Rev. (2023) 1–48, https://doi.org/10.1080/09506608.2022.2145747.
[30] F. Lo Monte, L. Repesa, D. Snoeck, H. Doostkami, M. Roig-Flores, S.J.P. Jackson, A. B. Alvarez, M. Nasner, R.P. Borg, C. Schröfl, M. Giménez, M.C. Alonso, P. Serna, N. De Belie, L. Ferrara, Multi-performance experimental assessment of autogenous and crystalline admixture-stimulated self-healing in UHPFRCCs: validation and reliability analysis through an inter-laboratory study, Cem. Concr. Compos. 145 (2023), https://doi.org/10.1016/j.cemconcomp.2023.105315.
[31] T.H. Ahn, D.J. Kim, S.H. Kang, Crack self-healing behavior of high performance fiber reinforced cement composites under various environmental conditions, in: Earth Sp. 2012 - Proc. 13th ASCE Aerosp. Div. Conf. 5th NASA/ASCE Work. Granul. Mater. Sp. Explor., 2012, https://doi.org/10.1061/9780784412190.068.
[32] Y.-S. Wang, H.-S. Lee, R.-S. Lin, X.-Y. Wang, Effect of silicate-modified calcium oxide-based expansive agent on engineering properties and self-healing of ultra-high-strength concrete, J. Build. Eng. 50 (2022), 104230, https://doi.org/10.1016/j.jobe.2022.104230.
[33] F. Lo Monte, L. Ferrara, Self-healing characterization of UHPFRCC with crystalline admixture: experimental assessment via multi-test/multi-parameter approach, Construct. Build. Mater. 283 (2021), 122579, https://doi.org/10.1016/j.conbuildmat.2021.122579.
[34] A. de Souza Oliveira, O. da Fonseca Martins Gomes, L. Ferrara, E. de Moraes Rego Fairbairn, R.D. Toledo Filho, An overview of a twofold effect of crystalline admixtures in cement-based materials: from permeability-reducers to self-healing stimulators, J. Build. Eng. 41 (2021), https://doi.org/10.1016/j.jobe.2021.102400.
[35] E. Cuenca, S. Rigamonti, E. Gastaldo Brac, L. Ferrara, Crystalline admixture as healing promoter in concrete exposed to chloride-rich environments: experimental study, J. Mater. Civ. Eng. 33 (2021), 04020491, https://doi.org/10.1061/(asce)mt.1943-5533.0003604.
[36] E. Cuenca, A. Mezzena, L. Ferrara, Synergy between crystalline admixtures and nano-constituents in enhancing autogenous healing capacity of cementitious composites under cracking and healing cycles in aggressive waters, Construct. Build. Mater. 266 (2021), 121447, https://doi.org/10.1016/j.conbuildmat.2020.121447.
[37] S. Al-Obaidi, M. Davolio, G. Recchia, F. Lo Monte, L. Ferrara, How does self-healing under sustained loadings in aggressive water affect the constitutive response of a UHPFRC? Spec. Collect. SHCC5, Springer, RILEM Bookseries. 39 (2023) 1–10.
[38] E. Cuenca, L. D'Ambrosio, D. Lizunov, A. Tretjakov, O. Volobujeva, L. Ferrara, Mechanical properties and self-healing capacity of ultra high performance fibre reinforced concrete with alumina nano-fibres: tailoring ultra high durability concrete for aggressive exposure scenarios, Cem. Concr. Compos. 118 (2021), 103956, https://doi.org/10.1016/j.cemconcomp.2021.103956.
[39] E. Cuenca, F. Lo Monte, M. Moro, A. Schiona, L. Ferrara, Effects of autogenous and stimulated self-healing on durability and mechanical performance of UHPFRC: validation of tailored test method through multi-performance healing-induced recovery indices, Sustainability 13 (2021), 11386, https://doi.org/10.3390/su132011386.
[40] F. Lo Monte, L. Ferrara, Tensile behaviour identification in Ultra-High Performance Fibre Reinforced Cementitious Composites: indirect tension tests and back analysis of flexural test results, Mater. Struct. Constr. 53 (2020), https://doi.org/10.1617/s11527-020-01576-8.
[41] M. di Prisco, L. Ferrara, M.G.L. Lamperti, Double edge wedge splitting (DEWS): an indirect tension test to identify post-cracking behaviour of fibre reinforced cementitious composites, Mater. Struct. 46 (2013) 1893–1918, https://doi.org/10.1617/s11527-013-0028-2.
[42] L. Ferrara, V. Krelani, M. Carsana, A "fracture testing" based approach to assess crack healing of concrete with and without crystalline admixtures, Construct. Build. Mater. 68 (2014) 535–551, https://doi.org/10.1016/j.conbuildmat.2014.07.008.
[43] S. Al-Obaidi, P. Bamonte, M. Luchini, I. Mazzantini, L. Ferrara, Durability-based design of structures made with ultra-high-performance/ultra-high-durability concrete in extremely aggressive scenarios: application to a geothermal water basin case study, Infrastructure 5 (2020) 102, https://doi.org/10.3390/infrastructures5110102.
[44] E. Cuenca, A. Tejedor, L. Ferrara, A methodology to assess crack-sealing effectiveness of crystalline admixtures under repeated cracking-healing cycles, Construct. Build. Mater. 179 (2018) 619–632, https://doi.org/10.1016/j.conbuildmat.2018.05.261.
[45] K. Komloš, S. Popovics, T. Nürnbergerová, B. Babál, J.S. Popovics, Ultrasonic pulse velocity test of concrete properties as specified in various standards, Cem. Concr. Compos. (1996), https://doi.org/10.1016/0958-9465(96)00026-1.
[46] W. Zhong, W. Yao, Influence of damage degree on self-healing of concrete, Construct. Build. Mater. (2008), https://doi.org/10.1016/j.conbuildmat.2007.02.006.
[47] P. Li, W. Li, T. Yu, F. Qu, V.W.Y. Tam, Investigation on early-age hydration, mechanical properties and microstructure of seawater sea sand cement mortar, Construct. Build. Mater. (2020), https://doi.org/10.1016/j.conbuildmat.2020.118776.
[48] M. Khoshroo, A.A. Shirzadi Javid, A. Katebi, Effect of chloride treatment curing condition on the mechanical properties and durability of concrete containing zeolite and micro-nano-bubble water, Construct. Build. Mater. (2018), https://doi.org/10.1016/j.conbuildmat.2018.05.086.
[49] H. Li, N. Farzadnia, C. Shi, The role of seawater in interaction of slag and silica fume with cement in low water-to-binder ratio pastes at the early age of hydration, Construct. Build. Mater. (2018), https://doi.org/10.1016/j.conbuildmat.2018.07.091.
[50] D.-Y. Yoo, J.Y. Gim, B. Chun, Effects of rust layer and corrosion degree on the pullout behavior of steel fibers from ultra-high-performance concrete, J. Mater. Res. Technol. 9 (2020) 3632–3648, https://doi.org/10.1016/j.jmrt.2020.01.101.
[51] D.-Y. Yoo, W. Shin, B. Chun, N. Banthia, Assessment of steel fiber corrosion in self-healed ultra-high-performance fiber-reinforced concrete and its effect on tensile performance, Cement Concr. Res. 133 (2020), 106091, https://doi.org/10.1016/j.cemconres.2020.106091.
[52] E. Cuenca, L. Ferrara, Fracture toughness parameters to assess crack healing capacity of fiber reinforced concrete under repeated cracking-healing cycles, Theor. Appl. Fract. Mech. 106 (2020), 102468, https://doi.org/10.1016/j.tafmec.2019.102468.
[53] Z. Jiang, W. Li, Z. Yuan, Influence of mineral additives and environmental conditions on the self-healing capabilities of cementitious materials, Cem. Concr. Compos. 57 (2015) 116–127, https://doi.org/10.1016/j.cemconcomp.2014.11.014.
[54] E. Cuenca, P. Serna, Autogenous self-healing capacity of early-age ultra-high-performance fiber-reinforced concrete, Sustainability 13 (2021) 3061, https://doi.org/10.3390/su13063061.
[55] P. Escoffres, C. Desmettre, J.-P. Charron, Effect of a crystalline admixture on the self-healing capability of high-performance fiber reinforced concretes in service conditions, Construct. Build. Mater. 173 (2018) 763–774, https://doi.org/10.1016/j.conbuildmat.2018.04.003.
[56] S. Kim, S. Choi, D.Y. Yoo, Surface modification of steel fibers using chemical solutions and their pullout behaviors from ultra-high-performance concrete, J. Build. Eng. (2020), https://doi.org/10.1016/j.jobe.2020.101709.
[57] N.R. Buenfeld, J.B. Newman, The development and stability of surface layers on concrete exposed to sea-water, Cement Concr. Res. (1986), https://doi.org/10.1016/0008-8846(86)90046-3.
[58] S. Alobaidi, S. He, E. Schlangen, L. Ferrara, Effect of matrix self-healing on the bond-slip behavior of micro steel fibers in ultra high-performance concrete, Submitt. to Mater. Struct. (2023), https://doi.org/10.21203/rs.3.rs-2841443/v1.
[59] M. Qian, Y. Zuo, Z. Chen, X. Yin, Y. Liu, W. Yang, Y. Chen, Crystallization of CaCO3 in aqueous solutions with extremely high concentrations of NaCl, Crystals 9 (2019) 647, https://doi.org/10.3390/cryst9120647.
[60] L. Fernández-Díaz, Á. Fernández-González, M. Prieto, The role of sulfate groups in controlling CaCO3 polymorphism, Geochem. Cosmochim. Acta 74 (2010) 6064–6076, https://doi.org/10.1016/j.gca.2010.08.010.
[61] P. Bots, L.G. Benning, J.D. Rodriguez-Blanco, T. Roncal-Herrero, S. Shaw, Mechanistic insights into the crystallization of amorphous calcium carbonate (ACC), Cryst. Growth Des. (2012), https://doi.org/10.1021/cg300676b.